RESEARCH ARTICLE

Macromolecular Chemistry and Physics
www.mcp-journal.de

Microscopic Characterization of Poly(Sulfur Nitride)

*Elkin Amado, Nazmul Hasan, Karsten Busse, and Jörg Kressler**

The morphology of poly(sulfur nitride) (SN_x) in bulk crystals and in thin films is investigated by grazing incidence wide-angle X-ray scattering (GI WAXS) and atomic force microscopy (AFM). SN_x crystals are grown in S_2N_2 crystals by topochemical solid-state polymerization and thin SN_x films are prepared by sublimation/repolymerization of SN_x or by mechanical deformation of crystals onto silicon substrates. Details of the crystallographic orientation of two different thin films are observed by GI WAXS. PeakForce Tunneling (PF-TUNA) atomic force microscopy provides information on the electrical conductivity of SN_x crystal together with its morphology in the nm range. The current–voltage (*I–V*) curves show ohmic behavior indicating the metallic nature of SN_x.

1. Introduction

The first synthesis of a material with similarities to poly(sulfur nitride) (SN_x) was carried out already in 1906 by O. C. M. Davis reacting tetrasulfur tetranitride (S_4N_4) with SbF_5 or MoF_5 in solution to receive blue colored crystals.[1] F. P. Burt synthesized for the first time SN_x when studying the sublimation of S_4N_4 over silver gauze in 1910.[2] This is still the standard synthetic procedure where S_4N_4 vapor converts in the presence of silver wool (silver sulfide) at elevated temperatures in vacuum to S_2N_2 which polymerizes slowly at room temperature to blue films or golden appearing crystals of SN_x in reflected light.[3] The polymeric character of SN_x, its diamagnetism, and its electrical conductivity were first summarized by Goehring and Voigt.[4,5] SN_x is unique in the field of synthetic polymers as it has the conductivity of metals at room temperature, at normal pressure, and without doping in the range of $1 - 4\times10^3$ S cm^{-1} which increases by a factor of 10^2 at 4.2 K.[6–8] Most common conductive polymers as poly(acetylene) or poly(aniline) are semiconductors after doping.[9,10] Furthermore, SN_x is the only synthetic polymer which shows superconductivity. The critical temperature is below 0.3 K for SN_x crystals,[11,12] whereas superconductivity in thin films could not be observed.[13] SN_x played an important role for the early studies on conductive polymers by Heeger and MacDiarmid.[14] The optical, magnetic, and electrical properties of SN_x are tightly related to its crystallization.[15,16] All synthetic procedures and physical properties of SN_x were extensively reviewed by Banister and Gorrell in 1998.[17]

Here, the morphology and the electrical conductivity of SN_x crystals are studied by various atomic force microscopy (AFM) techniques for the first time. Furthermore, grazing incidence wide-angle X-ray scattering (GI WAXS) measurements are employed for the first time for the characterization of thin SN_x films. These thin films were prepared by mechanical deformation or by vaporization/repolymerization of SN_x crystals onto silicon substrates.

2. Result and Discussion

2.1. SN_x Crystals in Bulk Samples

Figure 1 shows polarized optical microscopy (POM) images of typical SN_x crystals synthesized by topochemical solid-state polymerization of S_2N_2 in the crystalline state.[18,19]

The golden lustrous crystal depicted in Figure 1a indicates that the main polymer chain orientation is vertical along with the direction of the electric field vector of the polarized light.[20,21] This image shows already two main features of SN_x crystals: i) The crystals are formed by fibers along the main polymer chain direction, ii) they are not single crystals and show frequently a macroscopic twinning. As will be discussed in more detail below, also microscopic twinning cannot be excluded under any polymerization conditions in the S_2N_2 solid state.[22] Thus, earlier reports on the formation of large SN_x single crystals are not correct and the formation of single crystal-like domains in SN_x samples is limited to the nm range. The fiber formation is caused by the mismatch of the unit cell parameters of S_2N_2 crystals and SN_x crystals. Details of the crystalline structures are shown in **Scheme 1**.

The S_2N_2 unit cell according to Cohen et al.[18] is monoclinic with the dimensions $a = 4.485$ Å, $b = 3.767$ Å, and $c = 8.452$ Å and the monoclinic angle $\beta = 106.4°$ at −130°C. The cell is occupied by two S_2N_2 molecules in $P2_1/c$ space group (Scheme 1a). The SN_x unit cell according to Cohen is a monoclinic unit cell with the lengths $a = 4.153$ Å, $b = 4.439$ Å, and $c = 7.637$ Å and the monoclinic angle $\beta = 109.7°$ at room temperature (also called β-SN_x phase). The cell is occupied by two antiparallel SN_x chains in $P2_1/c$ space group (Scheme 1b). During synthesis, the SN_x *b*-direction (former S_2N_2 *a*-direction) becomes the chain axis, the cell volume decreases by 7%, and the *c** direction ($= c \sin(\beta)$) shrinks by 11%.[23] This strong decrease of the

E. Amado, N. Hasan, K. Busse, J. Kressler
Department of Chemistry
Martin Luther University Halle-Wittenberg
Halle (Saale) D-06120, Germany
E-mail: joerg.kressler@chemie.uni-halle.de

DOI: 10.1002/macp.202100113

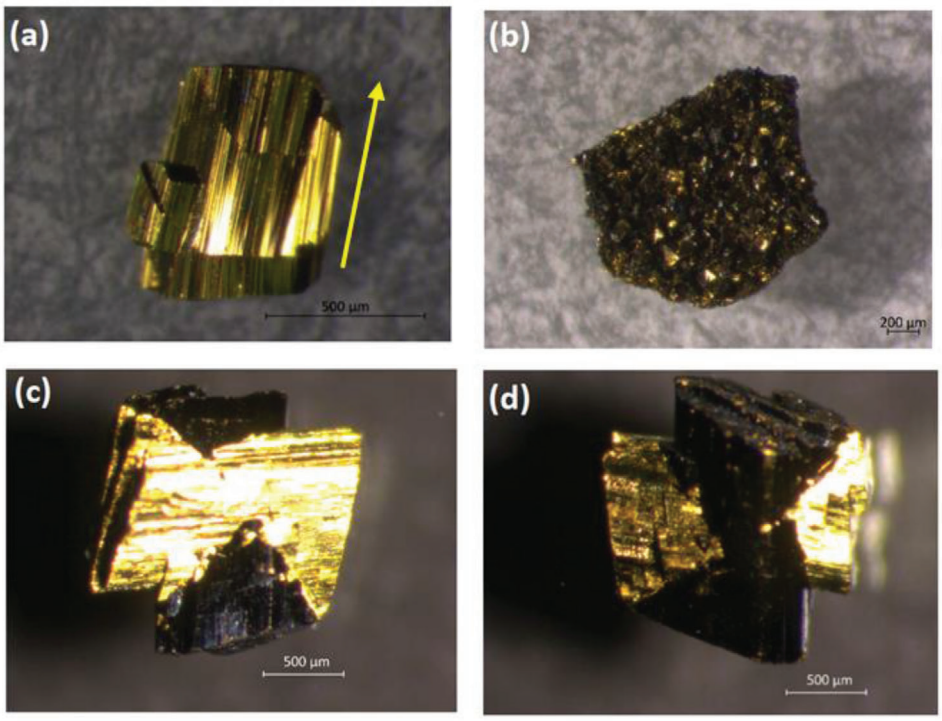

Figure 1. POM images: a) A typical SNx crystal, with the main fiber direction indicated by a yellow arrow. The light is vertically polarized. b) Agglomerate of small SN_x crystals. c) A SN_x crystal observed by horizontally polarized light. d) The same crystal rotated clockwise by 90°.

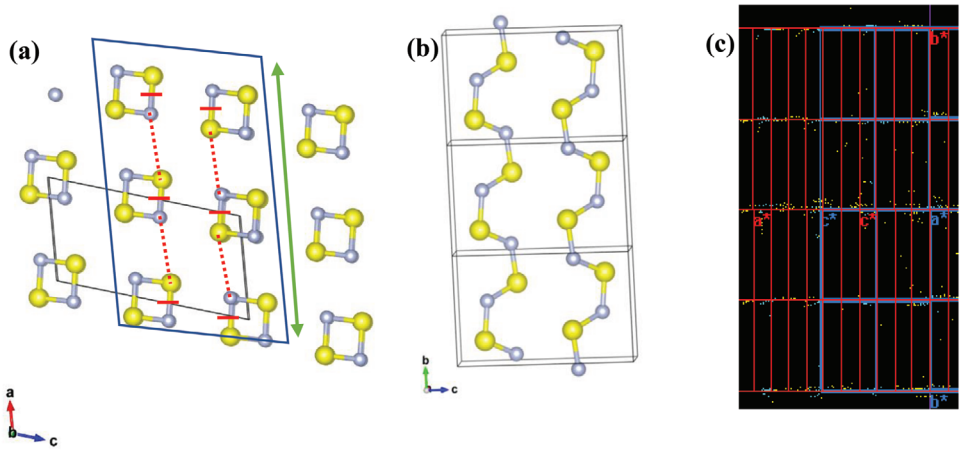

Scheme 1. Solid state polymerization: a) Ring opening of the S_2N_2 monomer. b) The final SN_x crystal (β-phase). All nitrogen atoms are gray and the sulfur atoms are yellow. Red bars indicate the ring opening and dotted lines the formation of new bonds. The green arrow is the growth direction of the polymer chain. A growth in *c* direction is rather unlikely, due to a larger distance and molecular tilt in S_2N_2 *b* direction, which is not visible in this projection. c) WAXS pattern of a SN_x crystal showing a highly oriented *b**-direction and a broad distribution of *a** and *c** directions in the corresponding horizontal plane. Unit cells in reciprocal space for one orientation (blue) and its ($\bar{1}$01) twin (red) are added to the pattern.

length perpendicular to the chain direction leads to the formation of microfibrillar crystallites.[22] Even these bundles are instable structures and can be separated into individual fibers by mechanical deformation. Nevertheless, the *b*-direction is uniform along the crystallite (Scheme 1c), with deviations of ± 5%.[24] The twin formation is the direct result of the S_2N_2 crystallization, as both formed polymer chains depicted in Scheme 1 are slightly tilted along the growth direction. For the final SN_x crystal, every second chain must rotate around their axis to obtain the final position. Statistically, positive rotation of first or negative rotation of second chain can appear with the same probability, which leads to micro-twinning. This process is the reason, why the SN_x single crystals appear only in the nanometer dimension as observed by transmission electron microscopy.[25] Another example for macro-twinning is given in Figure 1c,d. Here, the twins are growing nearly perpendicular to each other with respect to

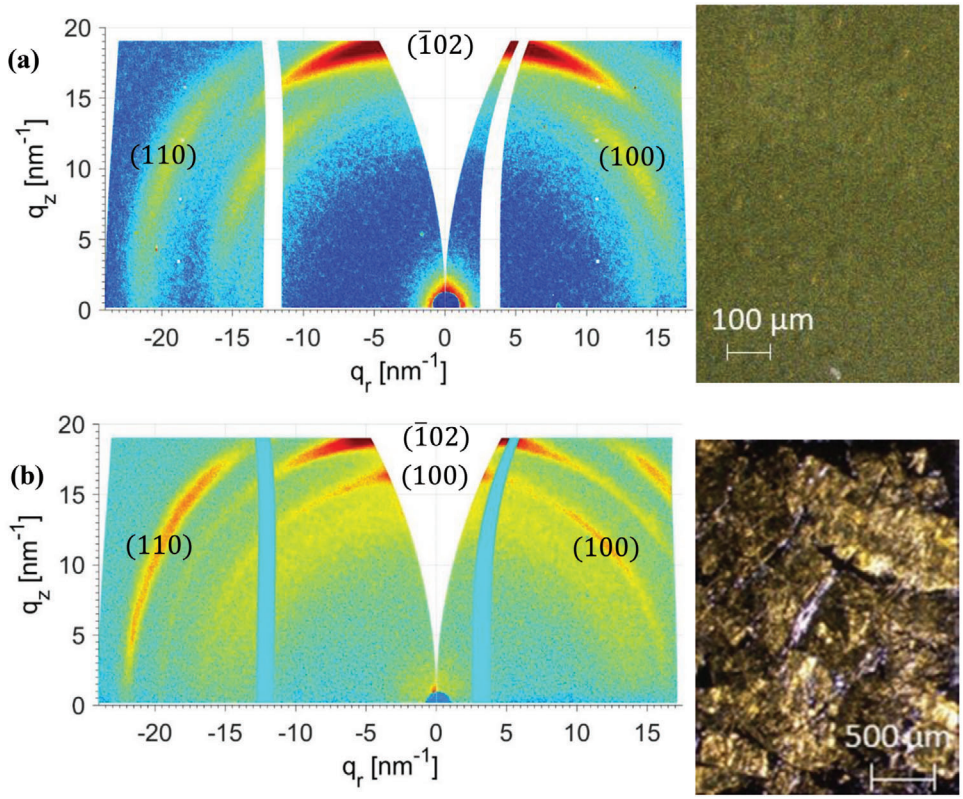

Figure 2. GI-WAXS and light microscopy photographs of a) thin film of SN_x prepared by sublimation of SN_x crystals and repolymerization from the vapor phase and b) mechanically oriented SN_x crystals pressed to a thin film.

their main fiber axis. This explains their golden and black/blue appearance. Rotating the crystals by 90° shows clearly their polymer chain orientation. Finally, Figure 1b shows a typical agglomerate of small SN_x crystals which grow at the cooling finger where S_2N_2 crystallizes from the gas flow during SN_x synthesis. The solid state polymerization itself takes ≈6 weeks at room temperature.

2.2. SN_x in Thin Films

A SN_x thin film on silicon was prepared by sublimation/repolymerization of a SN_x crystal (see experimental part). The film is analyzed by GI WAXS to identify the spatial orientation of SN_x, depicted in **Figure 2**a. The dominating ($\bar{1}02$) reflection is in the vertical direction, i.e., the planar SN_x chains are arranged (almost) parallel to the surface. A deviation of ≈±5° from uniform orientation is due to twisting and twinning, usually observed even in small crystals,[24] but also a local granular structure is observed by light microscopy measurements (Figure 2a, right photograph). The other observed reflections are identified as (110) and (100) with contributions of (012) and (002), respectively, which cannot be distinguished due to the restricted resolution of GI WAXS measurements. The thickness of the layer was 530 nm measured by scanning electron microscopy.

The sublimated/repolymerized film is compared with a thin layer of SN_x obtained by pressing small SN_x crystals on a silicon wafer. In light microscopy, the surface shows a more heterogeneous structure (rafts) (Figure 2b, right photograph), mostly based on different crystal orientations before pressing them on the surface. Nevertheless, the dominating ($\bar{1}02$) reflection is in vertical direction, too. This means that the SN_x chains have the same spatial orientation. In contrast to the sublimated/repolymerized sample, the additional (110) reflection became more extended, and, at least for some measurements, the (100) reflection also appears partially in vertical direction. It is well known, that the usual SN_x β-phase can be transformed by shear forces to an α-phase with orthorhombic cell,[26] in which the two polymer chains in a unit cell deviate from a total planar structure and other crystallographic planes might become preferred horizontal layers. In our GI WAXS experiments, the resolution is not sufficient to distinguish between both unit cells and peak indexation is performed according to the original β-SN_x phase.

2.3. AFM measurements – Morphology and Conductivity

In order to understand the surface morphology of SN_x crystals in nm scale, AFM with various modes such as PeakForce Quantitative Nanomechanics (PF-QNM) and standard tapping has been performed.[27–32] **Figure 3** shows AFM height images taken in PF-QNM mode in two different sizes. The images depict the fibrillar nature of the SN_x crystal with various fiber diameters in the range of about 50 to 100 nm. These fibers stack parallel to one another[19] to form bundles with sizes ranging from ≈

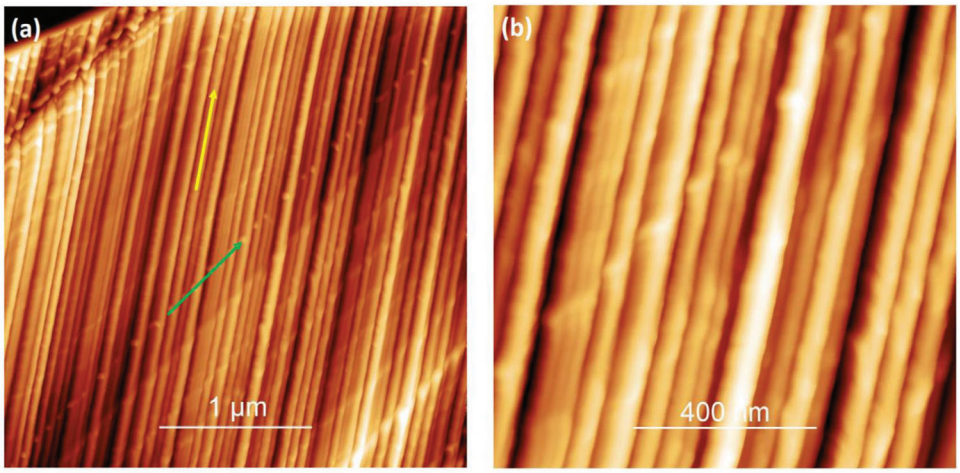

Figure 3. PF-QNM AFM height images of a SN_x crystal a) in 3×3 µm size with color scale from 17 to 40 nm and b) zoom in 1×1 µm size with color scale from 1 to 12 nm. The yellow arrow indicate the main fiber direction obtained by POM and the green arrow indicates a fiber direction which is not visible in POM.

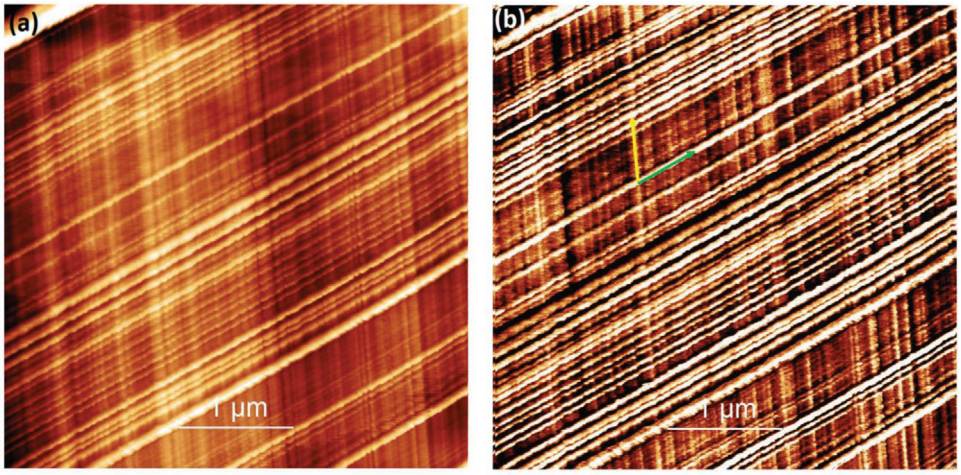

Figure 4. PF-QNM AFM images in 4×4 µm of a SN_x crystal. a) Height image with color scale from 2 to 11 nm and b) DMT Modulus map. The yellow and green arrows indicate the main fiber direction in agreement with POM and another fiber direction, respectively.

500 nm to 2 µm. By pressing a SN_x crystal with tweezer one can observe these bundles by optical microscopy. Scanning the fibers at a smaller scale as, e.g., below 500×500 nm shows a smooth surface without any evidence of surface structure (not shown here). The end of the fibers is also observed by AFM and can be seen in Figure 3a (at left-top corner). In addition to the main macroscopic fiber direction as observed by the POM (marked by yellow arrow), there is another fiber direction also present on the surface as indicated by a green arrow. This is hardly visible since the fiber growth is incomplete. Thus, we examined several SN_x crystals to observe more details about the different fiber directions. **Figure 4** shows AFM images of another crystal with two identified fiber directions. The main fiber direction obtained by POM is again indicated by a yellow arrow (Figure 4b). Another fiber direction that can only be seen by AFM is indicated by a green arrow. The angle between the two fiber directions is roughly 70° to 75°. As already discussed from X-ray data, the macroscopic SN_x crystals have nothing to do with classical 3D single crystals. But the polymer morphology might influence the electrical properties of SN_x as will be discussed below.

We also examined the surface of smaller SN_x crystals shown in Figure 1b. **Figure 5** shows the standard tapping mode AFM images using one of the crystals (golden entities in the image of Figure 1b). The surface morphology was found to be similar to that of a typical crystal, i.e., fibers with one main direction are found (Figure 5b,d, yellow arrows). This time we also observed the micro-twinning behavior[33] between the bundles of the fibers as indicated by several blue arrows in Figure 5b. Scanning this crystal at other places reveals another kind of surface structure (indicated by green arrows) growing in the same angle range of 70° to 75° with respect to the main fiber direction as depicted in Figure 5d.

The PF-TUNA AFM was used to demonstrate the electrical properties of the crystals. **Figure 6** shows the PF-TUNA AFM

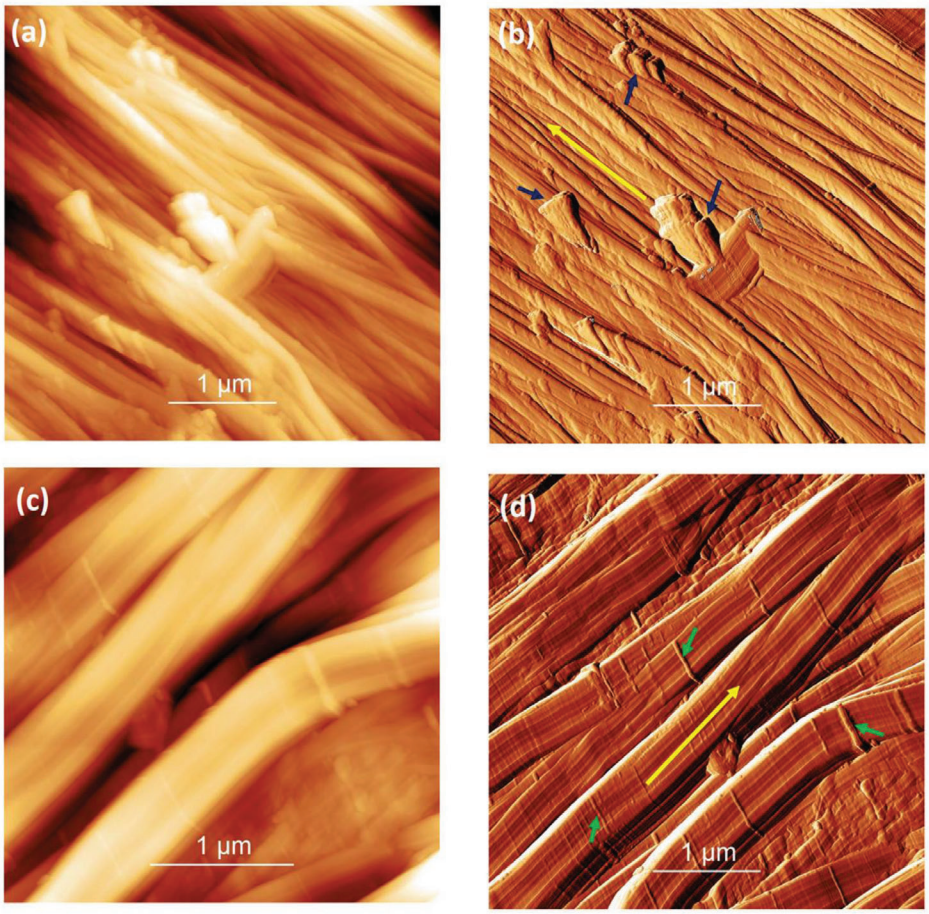

Figure 5. Tapping mode AFM images in 4×4 µm of small SN_x crystals. a,c) Height images with color scale between 70 to 470 nm and from 17 to 314 nm, respectively. b,d) Respective amplitude images.

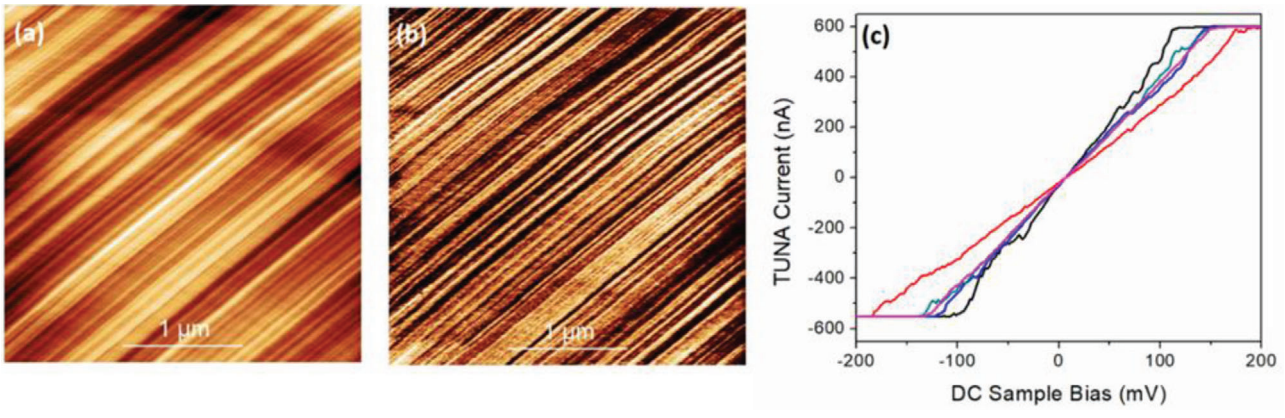

Figure 6. PF-TUNA AFM images of a SN_x crystal in 3×3 µm size. a) Height image with a color scale from 2 to 18 nm. b) TUNA Current map with a color scale from 6 to 65 pA. c) *I–V* curves taken at different spots of this sample.

images captured on another SN_x crystal. The height image (Figure 6a) shows the same fibrillar structure as mentioned previously. The TUNA current image in Figure 6b depicts the fiber conductivity in the range of 6 to 65 pA for a bias voltage of 100 mV. It should be noted the conductivity of the SN_x fibers is anisotropic,[17] i.e., the conductivity is pronounced along the fiber direction compared to the perpendicular fiber direction. The TUNA Current image (Figure 6b) is also showing a remarkably similar behavior (more bright contrast along the fiber direction). Since several factors influence the conductivity such as tip size

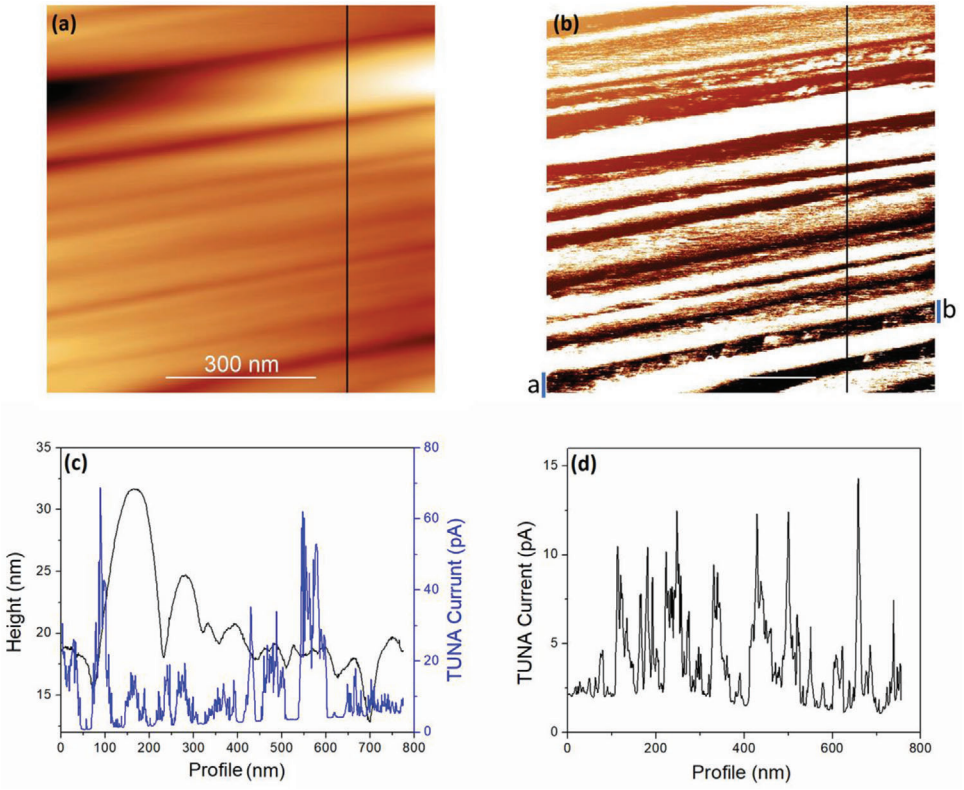

Figure 7. PF-TUNA AFM images in 775×775 nm of a SN_x crystal. a) Height image, b) TUNA Current map, c) Height and TUNA Current profile (vertical black lines), and d) TUNA Current profile from point a to b.

and geometry, surface roughness, applied force between tip and sample, and formation of a thin water layer on the sample,[34] it is difficult to draw simple conclusions from these measurements. A more detailed estimation is therefore done by measuring *I–V* curves at different spots of the crystal. Figure 6c shows 10 independent measurements at different locations of the crystal. The curves show that with the bias in the range of −200 to + 200 mV, the TUNA current increases linearly and is saturated (flat line) at around ± 600 nA. The linearity of the *I–V* curves indicates ohmic behavior, a very common phenomenon for different materials including metals.[35–37]

Finally, **Figure 7** depicts the PF-TUNA AFM images for another SN_x crystal recorded with bias voltage of 500 mV. A fibrillar structure can be seen from the height image (Figure 7a) along with two different fiber directions in TUNA Current map (Figure 7b). The underlying second fiber direction can be observed between the blue bars *a* and *b*. Several line profiles in vertical (black lines) and in horizontal direction between *a* and *b* are taken to understand the images better. The line scans of the height and the TUNA Current along the vertical lines (Figure 7a,b) are shown in Figure 7c. It can be noticed that there is a strong variation of the TUNA Current perpendicular to the fiber direction. Together with the height profile, it becomes clear that SN_x has a strong conductivity along the polymer chains and a reduced conductivity perpendicular to the fiber axis. It is also clear that the highest TUNA Current does not occur at the center of the fibers, i.e., the highest points of the height profiles. This is mostly due to the surface geometry, i.e., at the edge of the fibers, the AFM tip can collect current not only at the tip apex but also at the side of the tip surface, which results in increased conductivity. Similar results are reported for microcrystalline silicon samples measured by CAFM.[38] Figure 7d provides a nice example that the fibers perpendicular to the main fiber direction are also conductive. The line scan is taken between the blue bar *a* and *b* of Figure 7b. Since the phenomenon that many entities grow in a direction not in agreement the main bundle direction it can be assumed that SN_x is rather a 2D conductor rather a 1D conductor.

3. Conclusion

First GI WAXS measurements on thin SN_x films provide a detailed understanding of the polymer orientation in differently prepared samples. It makes a difference if the films were prepared by sublimation/repolymerization of SN_x crystals or by mechanical deposition of SN_x crystals onto the substrate. TUNA Current AFM seems to be a powerful tool to further investigate the conductivity in SN_x samples. It seems that SN_x is rather a 2D conductors and not a 1D conductor. This would contribute to the explanation of the superconductivity of SN_x crystals at low temperatures. It has been indicated by Ginzburg[39] that 2D superconductors exist whereas the 1D model of Little[40] for excitonic superconductivity along a polymer chain is not valid. This is supported by the fact that hitherto not a single synthetic polymeric superconductor has been found except SN_x.

4. Experimental Section

Synthesis of SN_x: SN_x was synthesized according to procedures given in literature.[18,19] In short, crystals of S_4N_4 were synthesized by reacting S_2Cl_2 with ammonia. Caution is necessary since S_4N_4 is explosive when heated or when subjected to mechanical stresses. Then S_4N_4 is decomposed over silver wool at elevated temperatures to S_2N_2 which polymerizes slowly at room temperature to SN_x. After 6 weeks metallic crystals were collected. The synthesized crystals were several times washed with ethanol, toluene, and finally chloroform. This is necessary in order to remove any impurities and residual S_2N_2. When these crystals are then stored in a glove box, they do not show any signs of degradation over years.

Thin Film Preparation: For pressed thin SN_x films, a single SN_x crystal was sandwiched between two layers of weighing paper and repeatedly flattened with a pestle until only thin flakes were left. The obtained discontinuous thin layer was glued to a silicon substrate for GI WAXS examination. Optical microscopy reveals that within a flake SN_x fibers are arranged parallel and lie approximately flat on the substrate plane. A typical raft-like morphology of the films is obtained. For thin SN_x films prepared by sublimation/repolymerization of SN_x crystals on silicon substrate, the silicon substrate was cleaned in concentrated sulfuric acid, 98% purity, for 20 min and thoroughly washed with deionized water. It was dried in a vacuum oven at 150°C, 1 mbar for 2.5 h. Then, the silicon substrate was glued to a stainless steel disc with colloidal silver. SN_x was vaporized at 145.0°C, 0.14 mbar and re-condensed onto the silicon substrate kept at 2.0°C. After 18 h the vaporization was stopped. The substrate was allowed to warm up to room temperature and stored in a glove box under nitrogen. The layer thickness was ≈530 nm, as measured by SEM. Optical microscopy reveals a granular structure evidenced at higher magnifications.

Atomic Force Microscopy (AFM): AFM measurements were performed with a MultiMode 8 instrument from Bruker (Santa Barbara, USA). SN_x crystals were initially examined with optical microscopy to identify the fiber direction and to check the roughness of the surface. Crystals were mounted on a metal disc support with double-sided adhesive tape. Crystals were mounted with the fibers lying on the X-Y plane. For conductivity measurements, colloidal silver paint was used to contact the crystal to the metal disc. Three different imaging modes were used. High-resolution images were captured in PeakForce Quantitative Nanomechanics (QNM) tapping mode with the PeakForce-HIRS-F-A and ScanAsyst-Fluid+ probes with a resonance frequency of 150–165 kHz and spring constant in the range 0.35–0.7 N m^{-1}. The local current–voltage characteristic of the crystals (*I–V* curve) was investigated with the PeakForce tunneling (PF-TUNA) mode, which measures local tunneling currents. Basically, a DC voltage bias is applied between the tip and the sample and the resulting current is measured. For these measurements, an SCM-PIT-V2 conductive probe with a spring constant of 3 N m^{-1} and a resonant frequency of 75 kHz was used. The DC bias voltage was in the range of 100 to 500 mV. The available voltage range for recording *I–V* curves is limited to −200 to +200 mV. All of the AFM measurements were carried out far below the resonance frequency of the cantilevers, i.e., with 1–2 kHz oscillation in air. The standard tapping mode images were recorded by a Mikromash NSC15 cantilever with a spring constant of 40 N m^{-1} and a resonance frequency of 325 kHz. Images were taken with lateral resolutions of 512 to 1024 pixels at a scanning speed of 0.3–0.8 Hz. The software program Gwyddion was used to process the AFM images.

Grazing Incidence Wide Angle X-Ray Scattering (GI WAXS): GI WAXS measurements were performed with a SAXSLAB laboratory setup (RetroF) equipped with an AXO microfocus source and monochromator for Cu K_α radiation ($\lambda = 0.154$ nm). 2D scattering patterns are recorded using a DECTRIS PILATUS3R 300 K detector in vacuum at room temperature. The sample-detector distance was fixed at 1548 mm and an incident angle of 0.2° was chosen. The obtained data are converted according to literature.[41,42]

WAXS Measurements: WAXS measurements on SN_x crystals were taken with a STOE-IPDS diffractometer with MoKα radiation ($\lambda = 0.7103$ A) with graphite monochromator. The sample is placed on a glass filament and stepwise rotated during experiment.

Polarized Optical Microscopy (POM): Polarized optical microscopy investigations were performed with a stereo microscope SteREO Discovery (Carl Zeiss) equipped with a polarization filter as analyzer. Microscopy images were acquired in reflection, with magnifications between 1.25x and 8x. A cold-light source CL-1500-HAL (Carl Zeiss) equipped with a polarization filter was used as a source of polarized light.

Acknowledgements

This work was supported by Deutsche Forschungsgemeinschaft (Project B07 of SFB TRR 102, project number 189853844). AFM and GI-WAXS measurements were supported by Prof. Thomas Thurn-Albrecht within the SFB TRR 102.

Open access funding enabled and organized by Projekt DEAL.

Conflict of Interest

The authors declare no conflict of interest.

Data Availability Statement

Research data are not shared.

Keywords

GI WAXS, PF-TUNA AFM, poly(sulfur nitride)

Received: March 31, 2021
Revised: July 23, 2021
Published online: August 8, 2021

[1] O. C. M. Davis, *J. Chem. Soc., Trans.* **1906**, *89*, 1575.
[2] F. P. Burt, *J. Chem. Soc., Trans.* **1910**, *97*, 1171.
[3] P. Love, G. Myer, H. I. Kao, M. M. Labes, W. R. Junker, C. Elbaum, *Ann. N. Y. Acad. Sci.* **1978**, *313*, 745.
[4] M. Goehring, D. Voigt, *Naturwissenschaften* **1953**, *40*, 482.
[5] M. Goehring, D. Voigt, *Z. Anorg. Allg. Chem.* **1956**, *285*, 181.
[6] V. V. Walatka, M. M. Labes, J. H. Perlstein, *Phys. Rev. Lett.* **1973**, *31*, 1139.
[7] M. M. Labes, P. Love, L. F. Nichols, *Chem. Rev.* **1979**, *79*, 1.
[8] C. K. Chiang, M. J. Cohen, A. F. Garito, A. J. Heeger, C. M. Mikulski, A. G. MacDiarmid, *Solid State Commun.* **1976**, *18*, 1451.
[9] A. J. Heeger, *Rev. Mod. Phys.* **2001**, *73*, 681.
[10] A. G. MacDiarmid, *Angew. Chem., Int. Ed.* **2001**, *40*, 2581.
[11] R. L. Greene, G. B. Street, L. J. Suter, *Phys. Rev. Lett.* **1975**, *34*, 577.
[12] L. J. Azevedo, W. G. Clark, G. Deutscher, R. L. Greene, G. B. Street, L. J. Suter, *Solid State Commun.* **1976**, *19*, 197.
[13] W. Beyer, W. D. Gill, G. B. Street, *Solid State Commun.* **1978**, *27*, 343.
[14] T. M. Swager, *Macromolecules* **2017**, *50*, 4867.
[15] L. Pintschovius, *Colloid Polym. Sci.* **1978**, *256*, 883.
[16] T. T. Takaluoma, K. Laasonen, R. S. Laitinen, *Inorg. Chem.* **2013**, *52*, 4648.
[17] A. J. Banister, I. B. Gorrell, *Adv. Mater.* **1998**, *10*, 1415.
[18] M. C. Cohen, A. F. Garito, A. J. Heeger, A. G. MacDiarmid, C. M. Mikulski, M. S. Saran, J. Kleppinger, *J. Am. Chem. Soc.* **1976**, *98*, 3844.
[19] C. M. Mikulski, P. J. Russo, M. S. Saran, A. G. MacDiarmid, A. F. Garito, A. J. Heeger, *J. Am. Chem. Soc.* **1975**, *97*, 6358.
[20] W. Möller, H. P. Geserich, L. Pintschovius, *Solid State Commun.* **1976**, *18*, 791.

[21] P. M. Grant, R. L. Greene, G. B. Street, *Phys. Rev. Lett.* **1975**, *35*, 1743.
[22] S. Isoda, A. Uemura, S. Moriguchi, M. Ohara, K. I. Katayama, *Bull. Inst. Chem. Res., Kyoto Univ.* **1988**, *66*, 530.
[23] H. Müller, S. O. Svensson, J. Birch, Å. Kvick, *Inorg. Chem.* **1997**, *36*, 1488.
[24] R. H. Hoel, D. J. Dingley, *J. Mater. Sci.* **1982**, *17*, 2997.
[25] J. Stejny, J. Dlugosz, A. Keller, *J. Mater. Sci.* **1979**, *14*, 1291.
[26] R. H. Baughman, P. A. Apgar, R. R. Chance, A. G. MacDiarmid, A. F. Garito, *J. Chem. Phys.* **1977**, *66*, 401.
[27] A. Kwaśniewska, M. Świetlicki, A. Prószyński, G. Gładyszewski, *Polymers* **2021**, *13*, 244.
[28] S. S. Nair, C. Wang, K. J. Wynne, *Prog. Org. Coatings* **2019**, *126*, 119.
[29] K. Xu, W. Sun, Y. Shao, F. Wei, X. Zhang, W. Wang, P. Li, *Nanotechnol. Rev.* **2018**, *7*, 605.
[30] C. Li, M. Ostadhassan, S. Guo, T. Gentzis, L. Kong, *Fuel* **2018**, *233*, 894.
[31] M. E. Dokukin, I. Sokolov, *Langmuir* **2012**, *28*, 16060.
[32] K. Sweers, K. van der Werf, M. Bennink, V. Subramaniam, *Nanoscale Res. Lett.* **2011**, *6*, 270.
[33] C. D. Rosa, F. Auriemma, *Crystals and Crystallinity in Polymer*, Wiley, Hoboken, NJ, USA **2014**.
[34] L. Jiang, J. Weber, F. M. Puglisi, P. Pavan, L. Larcher, W. Frammelsberger, G. Benstetter, M. Lanza, *Materials* **2019**, *12*, 459.
[35] B. Bercu, W. Geng, O. Simonetti, S. Kostcheev, C. Sartel, V. Sallet, G. Lérondel, M. Molinari, L. Giraudet, C. Couteau, *Nanotechnology* **2013**, *24*, 415202.
[36] S. H. Mir, B. Ochiai, *J. Electrochem. Soc.* **2018**, *165*, B3030.
[37] Y. Shi, Y. Ji, F. Hui, M. Lanza, in *2015 10th Spanish Conf. on Electron Devices (CDE)*, IEEE, Piscataway, NJ **2015**, pp. 1–4.
[38] A. Fejfar, B. Rezek, J. Čermák, *in Quantitative Data Processing in Scanning Probe Microscopy* (Ed: P. Klapetek), Elsevier, Amsterdam, Netherlands **2018**, Ch. 10.
[39] V. T. Ginzburg, *Rev. Mod. Phys.* **2004**, *76*, 981.
[40] W. A. Little, *Phys. Rev.* **1964**, *134*, A1416.
[41] O. Dolynchuk, P. Schmode, M. Fischer, M. Thelakkat, T. Thurn-Albrecht, *Macromolecules* **2021**, *54*, 5429.
[42] K. Busse, C. Fuchs, N. Hasan, M. Pulst, J. Kressler, *Langmuir* **2018**, *34*, 12759.

